
Article:
Padam, K.S.R., Pereira, S.D., Kumar, N.A.N. orcid.org/0000-0002-1759-1500 et al. (1 more author) (2025) Natural antisense transcript-mediated regulation of HOXA10-AS in oral squamous cell carcinoma. J Oral Pathol Med. ISSN 0904-2512

https://doi.org/10.1111/jop.13613

Journal of Oral Pathology & Medicine

WILEY

Journal of Oral Pathology & Medicine

ORIGINAL ARTICLE OPEN ACCESS

Natural Antisense Transcript-Mediated Regulation of HOXA10-AS in Oral Squamous Cell Carcinoma

Kanaka Sai Ram Padam[1] | Satyajit Dey Pereira[1] | Naveena A. N. Kumar[2] | Raghu Radhakrishnan[3,4,5]

[1]Department of Cell and Molecular Biology, Manipal School of Life Sciences, Manipal Academy of Higher Education, Manipal, Karnataka, India | [2]Department of Surgical Oncology, Kasturba Medical College and Hospital, Manipal Academy of Higher Education, Manipal, Karnataka, India | [3]Department of Oral Pathology, Manipal College of Dental Sciences, Manipal, Manipal Academy of Higher Education, Manipal, Karnataka, India | [4]Academic Unit of Oral and Maxillofacial Pathology, School of Clinical Dentistry, University of Sheffield, Sheffield, UK | [5]Academic Unit of Oral Biology and Oral Pathology, Muscat, Wattayah, Sultanate of Oman

Correspondence: Raghu Radhakrishnan (raghu.ar@manipal.edu)

Received: 10 July 2024 | **Revised:** 29 December 2024 | **Accepted:** 22 January 2025

Funding: This work was supported by the DBT/Wellcome Trust India Alliance (Grant IA/CPHI/18/1/503927) awarded to Raghu Radhakrishnan.

Keywords: CUR | epigenetics | HOXA10 | HOXA10-AS | unmethylation

ABSTRACT

Background: The oncogenic role of *HOXA10-AS* and *HOXA10* in cancer has been well documented. However, the epigenetic role of *HOXA10* and the natural antisense-mediated regulation of *HOXA10-AS* in oral squamous cell carcinoma progression is not understood.

Methods: A total of 35 oral squamous cell carcinoma specimens and 35 adjacent normal clinical specimens were collected and categorized on the basis of their lymph node status. *HOXA10-AS* and *HOXA10* expression were analyzed using RT-qPCR. Methyl-capture sequencing was performed using lymph node-negative ($n = 6$) and lymph node-positive ($n = 5$) matched cases. The promoter activity of *HOXA10* was determined using a luciferase assay. ChIP-qPCR was performed to determine histone mark localization in the distal promoter region of *HOXA10*. A protein–protein interaction network of genome-wide antisense targets was constructed using StringDB, and functional enrichment was performed using the R package ClusterProfiler. Transient siRNA-mediated transfection was performed to target specific exons of the *HOXA10-AS* gene, followed by subsequent cell proliferation, cell cycle, and cell migration assays and validation of cancer signaling pathways through western blotting.

Results: *HOXA10-AS* and its antisense target *HOXA10* were significantly overexpressed in the lymph node-positive samples. The transcriptionally active distal promoter of *HOXA10* consists of a constitutively unmethylated CpG island region (CUR). H3K4me3, H3K27ac, and H3K27me3 histone mark deposition at the adjacent methylated loci of the distal promoter suggest the nature of euchromatin-driven regulation. Genome-wide mapping revealed 11 potential targets of *HOXA10-AS*. Targeted specific knockdown of *HOXA10-AS* exons significantly reduced the expression of *HOXA10* and deregulated its downstream targets, contributing to decreased cell cycle progression and epithelial-to-mesenchymal transition.

Conclusion: *HOXA10-AS* regulates the expression of *HOXA10* through a natural antisense-mediated mechanism and is epigenetically regulated by constitutively unmethylated marks in the distally enhancing promoter of *HOXA10*.

1 | Introduction

Oral cavity neoplasms, comprising cancers of the lip, anterior two-thirds of the tongue, gingiva, floor of the mouth, and buccal mucosa (ICD10, C00-C06), rank among the top cancers globally, with the estimated number of new cases increasing from 354 864 in 2018 to 377 173 in 2020, posing serious quality of life, economic, and psychological burdens on patients [1, 2]. Cancers of the mouth are significantly more prevalent in regions such as South Central Asia and Melanesia, where Papua New Guinea has the highest global incidence [1]. Major contributors to oral squamous cell carcinoma (OSCC) include tobacco, alcohol, and areca nut use, while human papillomavirus infections are emerging as significant risk factors among young people in North America and Europe [3].

Long-noncoding RNAs (lncRNAs) are a class of RNA molecules (>200 nucleotides in length) that do not encode functional proteins but play crucial roles in regulating gene expression at various levels, including transcription, posttranscriptional, and epigenetic modifications [4]. One of the intriguing mechanisms by which lncRNAs regulate genes involves NAT (natural antisense transcript)-mediated regulation. These NATs are RNAs transcribed from the opposite strand of a coding gene, producing a complementary RNA sequence [5]. Exploring the potential links between NAT-mediated regulation and homeobox (*HOX*) genes in OSCC could be an emerging area of interest, considering the importance of *HOX* clusters in gene regulation and development.

HOXA10-AS, also known as *HOXA-AS4*, is a lncRNA transcribed from the complementary strand of the homeobox A10 (*HOXA10*) gene, which is located within the *HOXA* gene cluster on human chromosome 7 (p15.2) [6]. *HOXA10-AS*, an antisense transcript complementary to *HOXA10* mRNA, has been implicated in regulating *HOXA10* expression and influencing cell differentiation and development processes, thus playing crucial roles in developmental biology and gene regulation [6]. Studies indicate that *HOXA10-AS* can regulate genes crucial for cancer development and progression, including those involved in cell cycle control, apoptosis, and epithelial–mesenchymal transition (EMT) [6–9].

HOXA10 promotes cell proliferation and cell cycle progression through *HDAC1* (histone deacetylase 1) activity in hepatocellular carcinoma [10]. Its overexpression is linked to the overall poor survival of patients diagnosed with ovarian clear cell adenocarcinoma [11] and oral cancer [12]. While the contributions of *HOXA10-AS* and *HOXA10* to cancer progression are increasingly recognized, the precise role of *HOXA10-AS* in driving OSCC remains poorly understood. This study aimed to understand the molecular mechanisms by which *HOXA10-AS* orchestrates tumor progression, revealing its potential as a pivotal regulator and therapeutic target for OSCC treatment.

2 | Materials and Methods

2.1 | Clinical Specimen Collection

The study included a cohort of 35 adjacent normal tissue samples and 35 tumor tissue samples (Table 1). Among the tumors, 18 were lymph node-negative (LN−) and 14 were lymph node-positive (LN+) OSCC cases categorized on the basis of the LN status, excluding cases where nodal involvement was classified as NX (regional lymph nodes cannot be assessed). The samples included were further grouped into Stage I ($n=3$), Stage II ($n=9$), Stage III ($n=9$), Stage IV ($n=11$), well-differentiated ($n=26$), and moderately differentiated ($n=9$) OSCC cases. We followed the 8th edition of the TNM classification [13]. All patients underwent surgery at Kasturba Medical College, Manipal, India, with prior informed consent following the regulations of the Institutional Ethics Committee (IEC: 348/2018). We excluded patients who were reported to be treated with neoadjuvant therapy before biopsy. Samples were only collected from patients who had not undergone radiotherapy or chemotherapy prior to the study. This study included only samples that were analyzed for both the *HOXA10* and *HOXA10-AS* genes.

2.2 | Gene Sequence Retrieval and Transcript Mapping

The gene sequences of *HOXA10* and its embedded lncRNA *HOXA10-AS*, located within the HOX gene cluster, were retrieved from the NCBI reference sequence database using the UCSC genome browser (https://genome.ucsc.edu/cgi-bin/hgGateway). The graphical representation of the biological sequences was illustrated using the Illustrator for Biological Sequences software developed by the Cuckoo Workgroup [14].

2.3 | Cell Culture Conditions

Normal oral primary gingival keratinocytes (PGKs) (ATCC PCS-200-014) were procured from ATCC and subcultured in dermal cell basal medium (ATCC PCS-200-030) with a keratinocyte growth kit (ATCC PCS-200-040) as supplements. The OSCC cell line CAL27 (ATCC CRL-2095) was maintained in DMEM supplemented with 10% fetal bovine serum (FBS), and SCC-9 (ATCC CRL-1629) was maintained in a 1:1 mixture of DMEM and Ham's F12 medium (Cat. No. AT140, HiMedia) supplemented with 400 ng/mL hydrocortisone and 10% FBS.

2.4 | Gene Expression Analysis

Total RNA was isolated from the PGK, CAL27, SCC-9, and patient samples using the mirVana miRNA Isolation Kit with phenol (Cat. No. AM1560; Invitrogen). One microgram of isolated total RNA was used as input for cDNA conversion using a high-capacity cDNA reverse transcription kit (Cat. No. 4374966, Applied Biosystems) following the manufacturer's instructions. Approximately 10 ng of converted cDNA was used as a template for real-time PCR using TaqMan Universal Master Mix II (Cat. No. 4440038; Applied Biosystems). TaqMan probes for *HOXA10* (Assay ID: Hs00601076_m1), *HOXA10-AS* (Assay ID: Hs04231577_s1), and beta-actin (*ACTB*) (Assay ID: Hs01060665_g1) were used (Invitrogen, Thermo Fisher Scientific). All experiments were performed in triplicate, and the standard error of the mean (SEM) was determined as a dispersion measure across the biological samples analyzed. The data were analyzed using the $2^{-\Delta\Delta Ct}$ method [15], and the fold change was calculated relative to the reference group and visualized using the ggplot2 R package.

TABLE 1 | Clinicopathological profile of $n = 35$ matched case and adjacent normal samples, categorized into groups based on tumor specific variables (IEC: 348/2018).

				Pathologic staging			
Group	**Sample size (*n*)**	**Gender**	**Median age**	**T**	**N**	**M**	**Site(s)**
Matched normal	35	M ($n = 29$)	52	—	—	—	Buccal mucosa, gingiva, tongue, alveolus
		F ($n = 6$)					
Tumor	35	M ($n = 29$)	52	T1	N0	M0	Buccal mucosa, tongue, gingiva, alveolus
				T2	N1		
		F ($n = 6$)		T3	N2		
				T4	N3		
Grade 1	26	M ($n = 21$)	51.5	T1	NX	M0	Buccal mucosa, gingiva, tongue
				T2	N0		
				T3	N1		
		F ($n = 5$)		T4	N2		
					N3		
Grade 2	9	M ($n = 8$)	55	T1	NX	M0	Buccal mucosa, tongue, alveolus
				T2	N0		
		F ($n = 1$)		T3	N1		
				T4	N2		
					N3		
LN (–)	18	M ($n = 15$)	57	T1	N0	M0	Buccal mucosa, gingiva, tongue
				T2			
		F ($n = 3$)		T3			
				T4			
LN (+)	14	M ($n = 11$)	50	T1	N1	M0	Buccal mucosa, gingiva, tongue, alveolus
				T2	N2		
		F ($n = 3$)		T3	N3		
				T4			
Stage I	3	M ($n = 3$)	49	T1	N0	M0	Tongue, buccal mucosa
		F					
Stage II	9	M ($n = 7$)	53	T2	N0	M0	Tongue, gingiva, buccal mucosa
		F ($n = 2$)					
Stage III	9	M ($n = 8$)	50	T3	N0	M0	Tongue, buccal mucosa
		F ($n = 1$)			N1		
					N3		
Stage IV	11	M ($n = 8$)	53	T4	N0	M0	Buccal mucosa, gingiva, tongue, alveolus
					N1		
		F ($n = 3$)			N2		
					N3		

2.5 | Methyl-Capture Sequencing (MC-Seq)

MC-seq was performed on a panel of LN− ($n=6$) and LN+ ($n=5$) matched samples. Briefly, 500 ng of genomic DNA was sheared (150–200 bp) using a Covaris S2 sonicator, followed by end repair, adenylation, ligation, and subsequent library preparation using the SureSelectXT Methyl-Seq Target Enrichment System (Agilent Technologies, Santa Clara, CA, USA) following the manufacturer's guidelines. The captured libraries were subjected to bisulfite conversion using the EZ DNA Methylation Gold Kit followed by amplification using PCR. The paired-end sequencing of the libraries was performed via an Illumina HiSeq X Ten sequencer for 150 cycles following the manufacturer's instructions. FastQC v0.11.3 [16] was used to assess the quality of the raw reads, which were processed via TrimGalore (v0.4.0, Babraham Bioinformatics, Babraham Institute, Cambridge, UK) to obtain high-quality reads. The data were aligned to the human genome (hg19) using Bismark [17] and CpG calling was performed. The CpG-specific base-level resolution in the OSCC patient samples ($n=11$) was analyzed to decipher the methylation trends. The constitutively unmethylated regions (CURs) [17] encompassed by a valley of DNA methylation (DMVs) [18] changes in the surrounding region were characterized by base-level CpG-specific resolution. CURs are defined as segments of DNA with a loss of methylation independent of the sample type. A strict cut-off of $<10\%$ was applied to the site-specific CpG signals within and between the case–control samples. Only the gene regions that met these criteria were chosen for further analysis. The pooled adjacent normal and tumor samples ($n=11$ each) are presented as an average with SEM and were visualized using the ggplot2 R package.

2.6 | TCGA-WGBS Analysis of the *HOXA10* Distal Promoter Region

The *HOXA10* gene was screened to capture unmethylated CpG locus-specific methylation changes across the distal promoter region (−6.3 kb upstream) using a stringent cut-off of $<10\%$ for site-specific CpG signals in case–control samples. Only the regions that met the filtering criteria were chosen for further analysis. The Genomic Data Commons (GDC) pancancer whole-genome bisulfite sequencing (WGBS) data set comprising 23 cancer types from The Cancer Genome Atlas (TCGA) was obtained from the UCSC Xena database [19] and analyzed via R programming.

2.7 | Luciferase-Based Promoter Activity Screen

The *HOXA10* promoter immediately upstream of the TSS (−1016 to +8 bp; HOXA10pGL3pro) and distal upstream (−6326 to −5419 bp from the TSS; HOXA10pGL3dp) were cloned and inserted into the KpnI and NheI/HindIII restriction sites upstream of the pGL3 basic vector (Promega) containing the firefly luciferase gene. Primers for the promoter region of interest were designed via Primer3 (https://primer3.ut.ee/). Details of the primers used in the study were tabulated (Table 2). CAL27 cells were cultured in 24-well plates at 65% confluence and 500 ng of each promoter construct was cotransfected with 500 pg of the Renilla luciferase reporter plasmid (pRL-SV40, Promega) using Lipofectamine 3000 (Invitrogen, Cat. No. L3000001). Briefly, the plasmid DNA and the transfection reagent were diluted with Opti-MEM I reduced serum media (Thermo Fisher Scientific, Cat. No. 31985–062) and transfected into CAL27 cells while they were maintained in reduced-serum conditions for 12 h. After 12 h of transfection, the transfection media was replaced with normal growth media and maintained for an additional 48 h. The empty pGL3 basic without a promoter served as a negative control and the pGL3 control (Promega) with constitutive firefly luciferase expression served as a positive control. Luminescence was measured using a Dual-Luciferase Reporter Assay System (Promega, Madison, Cat. No. E1910) with an FB12 Single Tube Luminometer (Berthold Technologies GmbH & Co. KG). These data were normalized to the internal control pRL-SV40 (FLuc/RLuc relative light units), and promoter activity was compared with that of the vehicle pGL3 basic vector. The results are represented as the average fold change in expression as relative light units derived from two biological replicates.

TABLE 2 | List of Primers and restriction sites used for targeted amplification using PCR.

Name	Detail	Sequence	RE	T_H (°C)	Size (bp)
HOXA10pGL3DP	Forward	CGATGGTACCTTCCTCTTTGTTTGCTG	KpnI-HF	56	907
	Reverse	CCATAAGCTTACCAATCACTTCTTGAGG	HindIII-HF		
HOXA10pGL3pro	Forward	GAGTGGTACCGCCAAAGCTAACAGGA	KpnI-HF	56	1024
	Reverse	TGCAGCTAGCAAACATGCTGAATACG	NheI_HF		
dpdel1	Forward	CATGGGTACCAACAAGGGCCCTCC	KpnI-HF	52	334
	Reverse	CCCGAAGCTTCTGCTATTGAGATCTC	HindIII-HF		
prodel2	Forward	AGCAGGTACCGGAACATAAAGCAGCG	KpnI-HF	60	528
	Reverse	AGCTGCTAGCCTGGATCTGGAACTGG	NheI_HF		
prodel3	Forward	GCACGGTACCCATAAACACCCCACTT	KpnI-HF	54	363
	Reverse	TGCAGCTAGCAAACATGCTGAATACG	Nhe-HF		

Note: Underlined sequences denote the incorporated restriction sites of the restriction enzymes (RE).

2.8 | Chromatin Immunoprecipitation

The primers used for chromatin immunoprecipitation followed by quantitative PCR (ChIP–qPCR) are listed in Table 3. Briefly, CAL27 cells were grown to 85% confluence in a 150 mm culture dish (2×10^7 cells). After the media were removed, the cells were washed twice with 1× PBS and fixed with 0.75% formaldehyde (Sigma–Aldrich, Cat. No. 252549) for 10 min at room temperature. Glycine was added to a final concentration of 125 mM to stop cross-linking, followed by a 5-min incubation. The cells were washed twice with ice-cold 1× PBS, scraped, and centrifuged for 5 min at 4°C at 1000*g*. ChIP lysis buffer (50 mM HEPES-NaOH (pH 7.5), 140 mM NaCl, 1 mM EDTA, 1% Triton X-100, 0.1% sodium deoxycholate, 0.1% SDS) supplemented with protease inhibitors was added to the pellet. The lysate was sonicated (VCX750, Sonics Inc., USA) for 8 min (1 s on/off cycles at 40% amplitude) and centrifuged at 8000*g* for 10 min at 4°C. Five percent of the total chromatin was used as an input. Immunoprecipitation was performed overnight with antibodies against H3K4me3 (Cell Signaling Technology, Cat. No. C42D8), H3K27ac (Cell Signaling Technology, Cat. No. D5E4), H3K27me3 (Cat. No. C36B11; Cell Signaling Technology, USA), and normal nonimmuno rabbit IgG (MerckMillipore, Cat. No. NI01) overnight with Protein A/G plus agarose beads (sc-2003; Santa Cruz). The immunoprecipitated lysate was briefly centrifuged at 2000*g* for 1 min at 4°C, and the pellet was washed with high-salt buffer (20 mM Tris-HCl pH 8, 500 mM NaCl, 0.1% SDS, 1% Triton-X-100, 2 mM EDTA), low-salt buffer (20 mM Tris-HCl pH 8, 150 mM NaCl, 2 mM EDTA, 1% Triton-X-100, 0.1% SDS), and KCl buffer (10 mM Tris-HCl pH 8, 1 mM EDTA, 1% sodium deoxycholate, 1% NP-40, 0.25 M KCl). Reverse crosslinking was performed by adding TE (25 mM Tris–HCl, 1 mM EDTA) buffer supplemented with proteinase K (20 μg/mL) and RNase A (10 μg/mL) at 55°C for 15 min, followed by incubation at 100°C for 15 min. Approximately 500 pg of IP DNA was used for qPCR. The fold enrichment was calculated relative to the mock IgG control (nonimmune normal rabbit IgG), and the data are presented as an average of three biological replicates with standard deviation (SD).

2.9 | Protein–Protein Interaction Network

HOXA10-AS is present on the positive strand and serves as a natural antisense to *HOXA10* on the negative strand of chromosome 7 (chr7 p15.2). To investigate the antisense potential of *HOXA10-AS* exons in other genes, we used the following method. Reverse-complemented *HOXA10-AS* exons were input into UCSC BLAT (BLAST-like alignment) [20] for alignment. We used the criteria of ≥ 20 bases and ≤ 2 mismatches for the query. The results were mapped to the hg19 genome to identify strand-specific genomic regions. Genes antisense to HOXA10-AS were then input into StringDB [21] for protein–protein interaction analysis with a confidence score > 0.4. Visualization was performed using Cytoscape [22].

2.10 | Functional Overrepresentation Analysis (ORA)

The downstream functional consequences of the protein–protein interactions of the *HOXA10-AS* target mRNAs were analyzed via Gene Ontology (GO) biological process (BP) and Kyoto Encyclopedia of Genes and Genomes (KEGG) pathway analyses [23] with the ClusterProfiler R package [24]. For ORA, the subset of *HOXA10-AS* target genes and their downstream protein–protein interactions were compiled as a query set. An adjusted p value (< 0.05) with the Bonferroni–Hochberg correction was used to determine statistical significance. Only the relevant BP categories and KEGG pathways are illustrated.

2.11 | Small-Interfering RNA (siRNA) Design and Transfection

siRNA duplexes targeting Exon 2 (sense: CUACCUAAAUC ACCGACCA; antisense: UGGUCGGUGAUUUAGGUAG) and Exon 3 (sense: GCGGCUCCUUUGCACCAUU; antisense: AAUGGUGCAAAGGAGCCGCC) of *HOXA10-AS* (ENST00000519935.1) along with a negative control siRNA (Silencer Select, Cat. No. 4390843) were purchased (Assay ID: n511472; n511473, Thermo Fisher Scientific). The siRNAs were diluted to 200 μM stock and 10 μM working concentrations in nuclease-free water. These siRNAs were designed to target exons of *HOXA10-AS* that are homologous in sequence to shared exons from alternate splicing events, facilitating effective knockdown of target *HOXA10-AS* expression in cells. CAL27 cells were seeded to 65% confluency in a 60 mm culture dish 1 day before siRNA transfection. Briefly, 25 nM each

TABLE 3 | List of primers designed for the ChIP–qPCR spanning the *HOXA10* distal promoter region.

Name		Sequence	T_m (°C)	Genomic coordinates (hg19)	Product size (bp)
DPRa	Forward	GAGAGAGTCTAGCCAGGAGGACTG	62.2	chr7:27219701-27219857 (–)	157
	Reverse	TAGCGGCGCATTCCAAATA	62.5		
DPRb	Forward	GGAATGCGCCGCTATAAA	59.8	chr7:27219611-27219714 (–)	104
	Reverse	AAGGAGAGAGGAGAGGATGTG	57.5		
DPRc	Forward	CATCCTCTCCTCTCTCCTTCT	56.7	chr7:27219503-27219629 (–)	127
	Reverse	CTTTGACATTGATCGGAAGT	55.2		
DPRd	Forward	GCATGATTCTTGGCCTTTGT	60.1	chr7:27219280-27219479 (–)	200
	Reverse	AAATCACTGCCAAGGGACAG	60.1		

of Exon 2-specific (siEx2), Exon 3-specific (siEx3), and pooled Exons 2 and 3 siRNAs (siEx23) in equimolar concentrations were diluted in Opti-MEM I reduced serum media (Thermo Fisher Scientific, Cat. No. 31985–062). Lipofectamine RNAiMAX transfection reagent (Thermo Fisher Scientific, Cat. No. 13778075) was used following the manufacturer's protocol. After incubation for 12 h, the media was replaced with regular growth media, and the cells were maintained for another 2 days followed by RNA and protein isolation for the validation of the knockdown. All experiments were performed in three biological replicates.

2.12 | Cell Proliferation Assay

CAL27 cells were initially seeded onto 10 cm culture dishes at 60%–65% confluence, and the following day, the cells were transiently transfected with siRNA targeting Exon 3 of *HOXA10-AS* under reduced serum-free conditions as described earlier. One day after transfection, 2000 cells per well were seeded into a 96-well plate on the initial day to assay the cell proliferation rate for 5 days, and readings were taken every day. Briefly, 10 μL of CCK-8 (Cat No. CK04-11, Dojindo) solution was added to each well, and the mixture was incubated for 4 h at 37°C. The absorbance of the dye at 450 and the 650 nm reference background was measured using a Varioscan Flash microplate reader (Cat. No. N06355, Thermo Fisher Scientific, USA). The data are illustrated as a line plot by taking the time in days on the *x*-axis versus the absorbance on the y-axis and represented as the average with the SD derived from three biological replicates.

2.13 | Wound Healing Assay

After 24 h of transfection, the *HOXA10-AS*-knockdown CAL27 cells and control cells were seeded onto a six-well culture dish in duplicate to the desired confluency of 95%. A vertical scratch was induced in the confluent culture dishes, and scratch imaging was performed on the initial day, which was recorded as 0 h. Migration was monitored every 12 h until the wound closed in either the test or the control. The data were analyzed as a percentage of wound closure over time, and the rate of cell migration (μm/h) was determined using the wound healing size tool [25] in ImageJ [26]. Two biological replicates of the experiments were performed.

2.14 | Cell Cycle Analysis

After transfection, the cells were grown in complete culture media for 2 days until they reached 60%–65% confluence. The cells were then trypsinized with 0.125% Trypsin-10 mM EDTA, washed with 1× PBS, fixed with 70% ethanol in 1× PBS, and incubated at 4°C overnight. The following day, the cells were treated with RNase (10 μg/mL) at 37°C, followed by incubation with propidium iodide (Cat. No. P4170, Sigma–Aldrich) at 4°C for 30 minutes. The cells were then processed for flow cytometry (CyFlow Space, Sysmex, Germany) analysis to estimate the different phases of cell progression. Two biological replicates of the experiments were performed.

2.15 | Western Blotting

After trypsinization, PGK, CAL27, SCC-9, and the transfected cells were washed in 1× PBS (pH 7.0) and lysed in RIPA lysis buffer (Santa Cruz Biotechnology, Cat. No. sc-24948A). A total of 20 μg of total protein was loaded onto a 10% SDS–polyacrylamide gel and transferred to a PVDF membrane (Bio-Rad, Cat. No. 1620177). The membranes were blocked with 5% bovine serum albumin (BSA) in Tris-buffered saline (TBS) containing 0.05% Tween-20 (1× TBST) for 1 h and incubated overnight with primary antibodies (Table S1) at 4°C. The following day, the membranes were rinsed (1× TBST) and incubated with secondary antibody at room temperature for 1 h. The membranes were washed in 1× TBS (pH 7.4) and developed with Clarity Western ECL Substrate (Cat. No. 1705061; Bio-Rad Laboratories) using the iBright CL1500 Imaging system (Cat. No. A44114; Thermo Fisher Scientific). All the experiments were performed in two biological replicates.

2.16 | Statistical Analysis

The Kruskal–Wallis test was used to assess variation among multiple independent groups when the data did not satisfy normality assumptions. For post hoc pairwise comparisons of nonparametric data, Dunn's test was applied with a focus on the chi-square (χ^2) statistic and adjusted p value (p). For parametric data, one-way ANOVA followed by Tukey's HSD test was used for multiple group comparisons, or Dunnett's test was applied for comparing treatment groups to a control group, reporting the F statistic (F), p value, and Studentized range (q) statistic where appropriate. A two-tailed paired t test was used to compare related groups, whereas a two-tailed unpaired t test was used for independent groups, which was determined on the basis of normality and sample size. Statistical analyses were performed using the R packages Rstatix and GraphPad Prism (version 8.0; GraphPad Software, Boston, USA), with significance set at $p < 0.05$.

3 | Results

3.1 | *HOXA10-AS* and *HOXA10*, Which Are Positioned Naturally Antisense to Each Other, Were Overexpressed

The *HOXA10-AS* transcript variant (ENST00000519935.1) consists of three exons, with the third exon being antisense to Exon 2 of the *HOXA10* transcript variant (ENST00000283921.5), which contains the *HOX* domain that functions as a transcription factor (Figure 1A). *HOXA10-AS* (2.55 ± 0.42, $\chi^2 = 22.85$, $t = 2.72$, $p = 0.006$) and *HOXA10* (1.86 ± 0.29, $\chi^2 = 15.69$, $t = 2.01$, $p = 0.043$) were significantly upregulated in OSCC samples compared with matched normal tissue samples ($n = 35$). Compared with those in normal samples, higher expression levels of *HOXA10-AS* (2.15 ± 0.37, $t = 2.64$, $p = 0.008$) and *HOXA10* (3.40 ± 0.65, $t = 3.58$, $p = 0.0003$) were detected in the lymph node-positive samples than in the lymph node-negative samples. *HOXA10-AS*, which is positioned as a NAT to *HOXA10*, showed similar expression patterns in the OSCC samples, suggesting NAT-mediated regulation (Figure 1B,C). Our findings

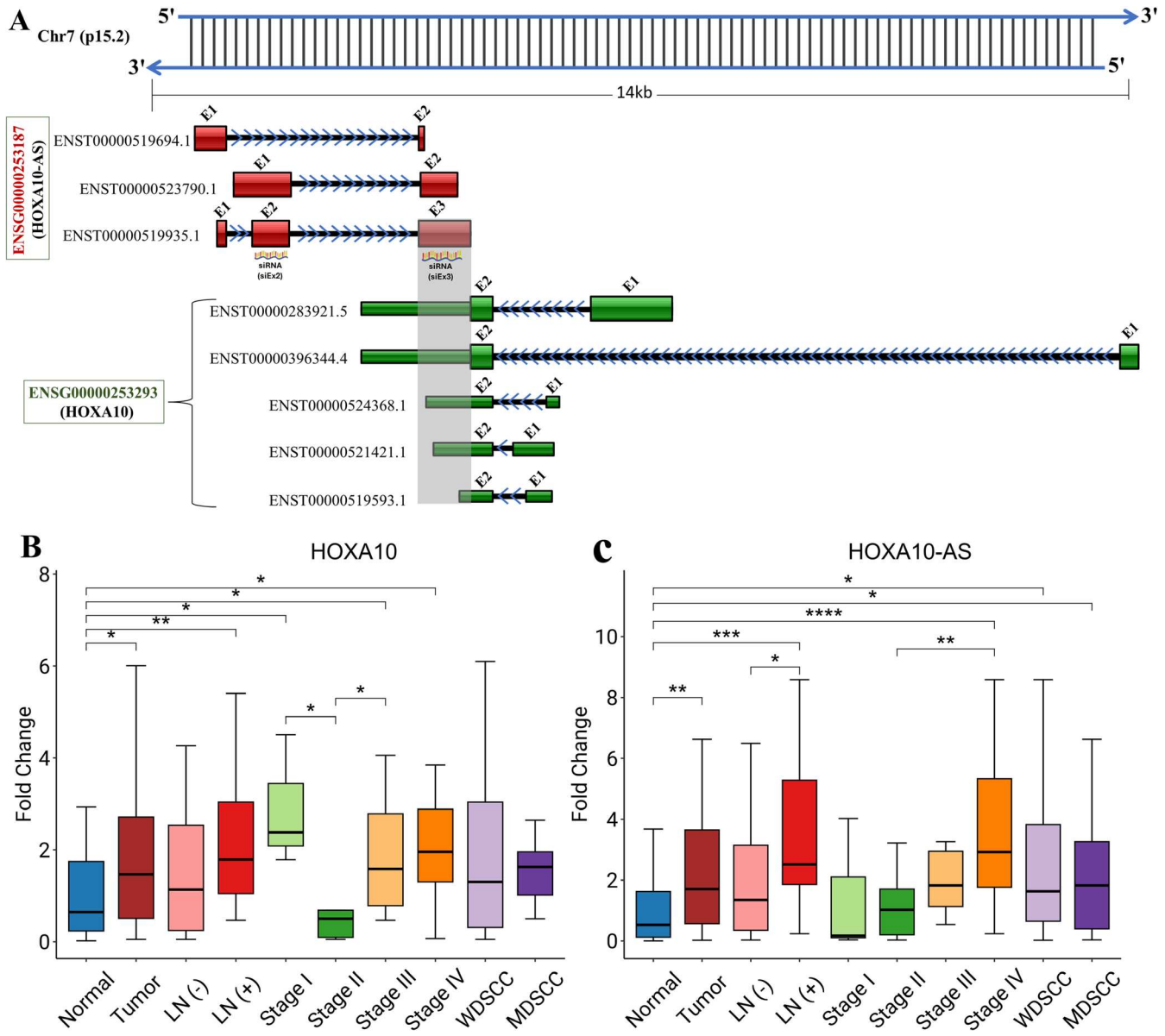

FIGURE 1 | The long noncoding RNA *HOXA10-AS* is a naturally occurring antisense of homeobox A10. (A) Schematic representation of *HOXA10-AS* on the forward strand and homeobox A10 transcripts on the antisense strand showing two canonical transcripts: Variant 1 (ENST00000283921.5, NCBI RefSeq-NM_018951.4) and variant 2 (ENST00000396344.4, NCBI RefSeq-NR_037939.2). Exon 3 of *HOXA10-AS* (ENST00000519935.1) complements Exons 2 and the 3′UTR of *HOXA10*. Noncanonical splice variants of both *HOXA10-AS* and *HOXA10* are also illustrated. (B) Gene expression profiles of *HOXA10* and (C) *HOXA10-AS* in normal ($n = 35$), LN (−) ($n = 18$), LN (+) ($n = 14$), Stage I ($n = 3$), Stage II ($n = 9$), Stage III ($n = 9$), Stage IV ($n = 11$), well-differentiated ($n = 26$), and moderately differentiated cases ($n = 9$). Only samples analysed for both genes were included. The experiments were performed in triplicate, and the data were analysed using the $2^{-\Delta\Delta Ct}$ method. Kruskal–Wallis ANOVA with post hoc Dunn's test was used to calculate the statistical significance (*$p < 0.05$; **$p < 0.01$; ***$p < 0.001$; ****$p < 0.0001$).

suggest a positive regulatory relationship between *HOXA10-AS* and *HOXA10* at the RNA level.

3.2 | First Exon Methylation of the Gene Inversely Regulates *HOXA10* Expression

The *HOXA10* gene showed nondifferential methylation patterns in both normal and tumor samples ($n = 11$ each), with locus-specific (hg19/chr7:27213492–27 213 626–1) altered methylation patterns observed in the first exon, likely due to the differential expression of *HOXA10* (Figure 2A,B). However, no significant differences were noted in the methylation of *HOXA10-AS* transcripts profiled between tumor and normal samples (Figure S1). Patient samples categorized by *HOXA10* expression levels ($n = 11$ each) presented an intermediate increase in CpG methylation (19.58% ± 0.78%) in the first exon, which coincided with decreased gene expression (Figure 2C,D). The CpG island located 6.3 kb upstream (hg19/chr7:27219413–27 219 738:-1) from the gene body was observed to be constitutively unmethylated in both normal (4.62% ± 1.31%) and tumor (4.91% ± 1.52%) samples (Figure 2E). This observation was consistent with TCGA pancancer WGBS data in normal (beta score: 0.019 ± 0.013) and tumor samples

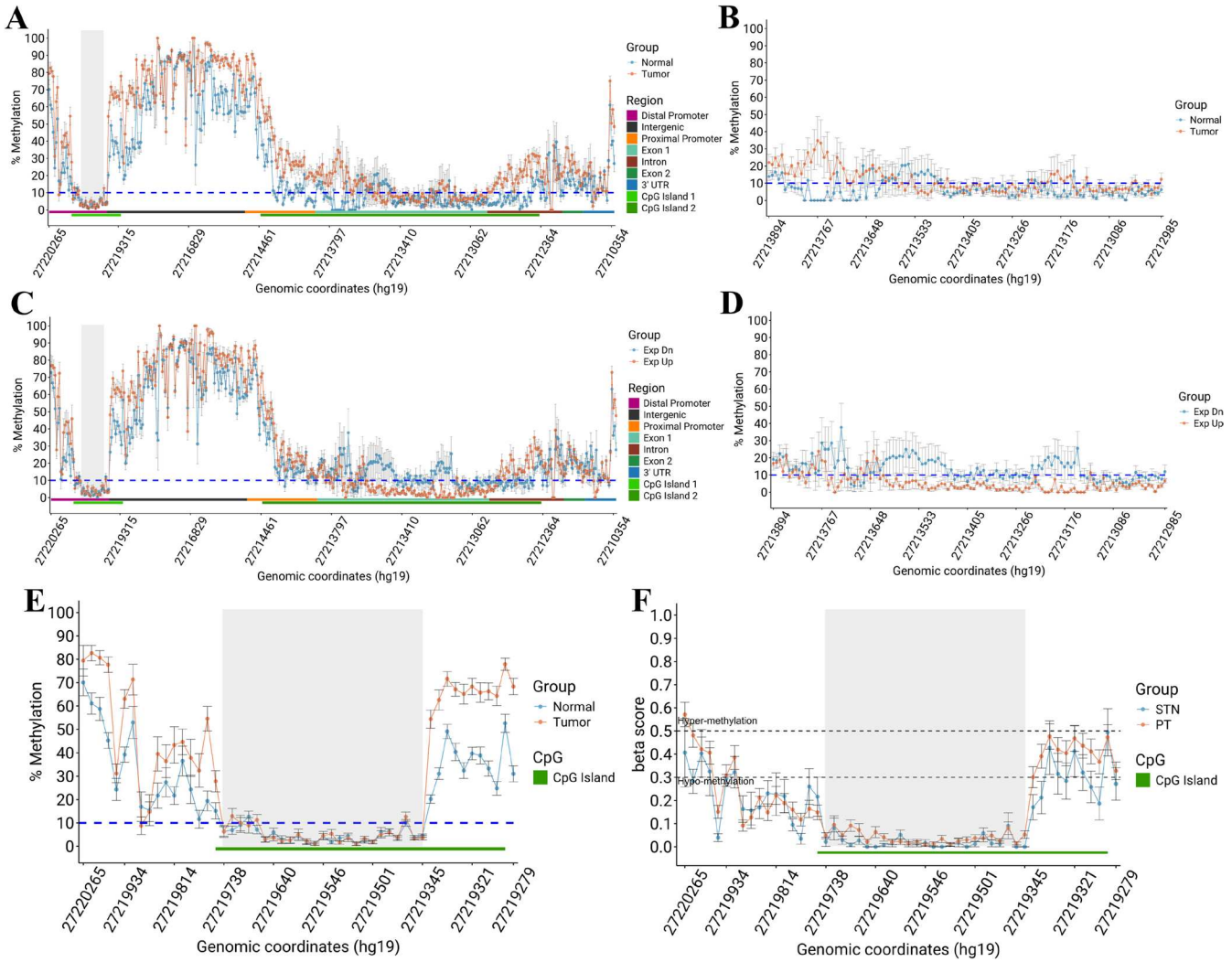

FIGURE 2 | Gene body methylation in the first exon and transcriptional repression of *HOXA10*. (A) Gene-wide and (B) first exonic methylation profiles of *HOXA10* in normal ($n = 11$) and tumor ($n = 11$) cases. (C) Trend of gene-wide methylation in OSCC tumors ($n = 11$) and normal controls ($n = 11$) and (D) exon 1-specific methylation profiles in patient samples categorized on the basis of *HOXA10* gene expression. (E) Methylation profile of the *HOXA10* distal promoter region (located −6.3 kb upstream of the gene body), analysed via MC-seq in case–control ($n = 11$) samples. A cut-off of $< 10\%$ was reported to indicate unmethylation (represented by the blue dashed line). (F) Methylation pattern of the *HOXA10* distal promoter region in WGBS datasets from the TCGA pancancer cohort ($n = 8$ normal, $n = 39$ primary tumors). A beta score of 0.5–0.7 indicates hypermethylation, whereas a beta score of 0.25–0.3 indicates hypomethylation. Exp Dn, downregulated expression; Exp Up, upregulated expression; PT, primary tumor; STN, normal solid tissue.

(0.038 ± 0.015) (Figure 2F). Similar patterns were observed in CAL27 cells, SCC-9 cells, and normal PGKs (Figure 3A), where the distal CpG island region of *HOXA10* exhibited distinct CUR marks. *HOXA10-AS* was significantly overexpressed in both CAL27 (79.83 ± 2.16, $t = 63.01$, $p = 0.0003$) and SCC-9 (24.05 ± 2.59, $t = 15.39$, $p = 0.0042$) cells. Concomitant overexpression of HOXA10 was noted in the OSCC cells CAL27 (56.91 ± 1.03, $t = 93.45$, $p = 0.0001$) and SCC-9 (31.34 ± 0.92, $t = 56.79$, $p = 0.0003$) compared with the PGKs (Figure 3B–D).

3.3 | Distal and Proximal Promoters Transcriptionally Regulate *HOXA10* Gene Expression

On the basis of our earlier observations of *HOXA10* methylation and gene expression in patients and cell lines, luciferase promoter constructs and ChIP–qPCR primers were designed (Figure 3E). The highest promoter activity ($F = 380.2$, $p = 0.0001$) was detected in the distal (HOXA10pGL3DP) and proximal (HOXA10pGL3pro) CpG island-rich regions. The promoter region nearest the TSS (prodel3) presented greater activity (1633.87 ± 80.49, $q = 30.69$, $p = 0.0001$, 0.0001) than the other deletion constructs (dpdel1; prodel2), which presented lower luciferase activity (66.32 ± 8.49, 49.82 ± 2.17, $q = 1.22$, 0.91, $p = 0.67$, 0.86) (Figure 3F). ChIP analysis ($F = 244.1$, $p = 0.0001$) of CAL27 cells revealed H3K27ac (12.04 ± 2.54 ac, $q = 5.49$, $p = 0.0009$) enrichment followed by H3K27me3 (21.58 ± 1.43, $q = 10.24$, $p = 0.0001$) enrichment in the DPRa region and H3K4me3 enrichment in the DPRb (82.25 ± 3.48, $q = 40.41$, $p = 0.0001$) and DPRd (24.57 ± 1.48, $q = 11.73$, $p = 0.0001$) regions, with reduced enrichment of euchromatin marks (H3K4me3; H3K27ac) in the DPRc (11.57 ± 3.45, 0.62 ± 0.30, $q = 5.27$, 0.18, $p = 0.001$, 0.99) region. Interestingly, DPRc is the region associated with the

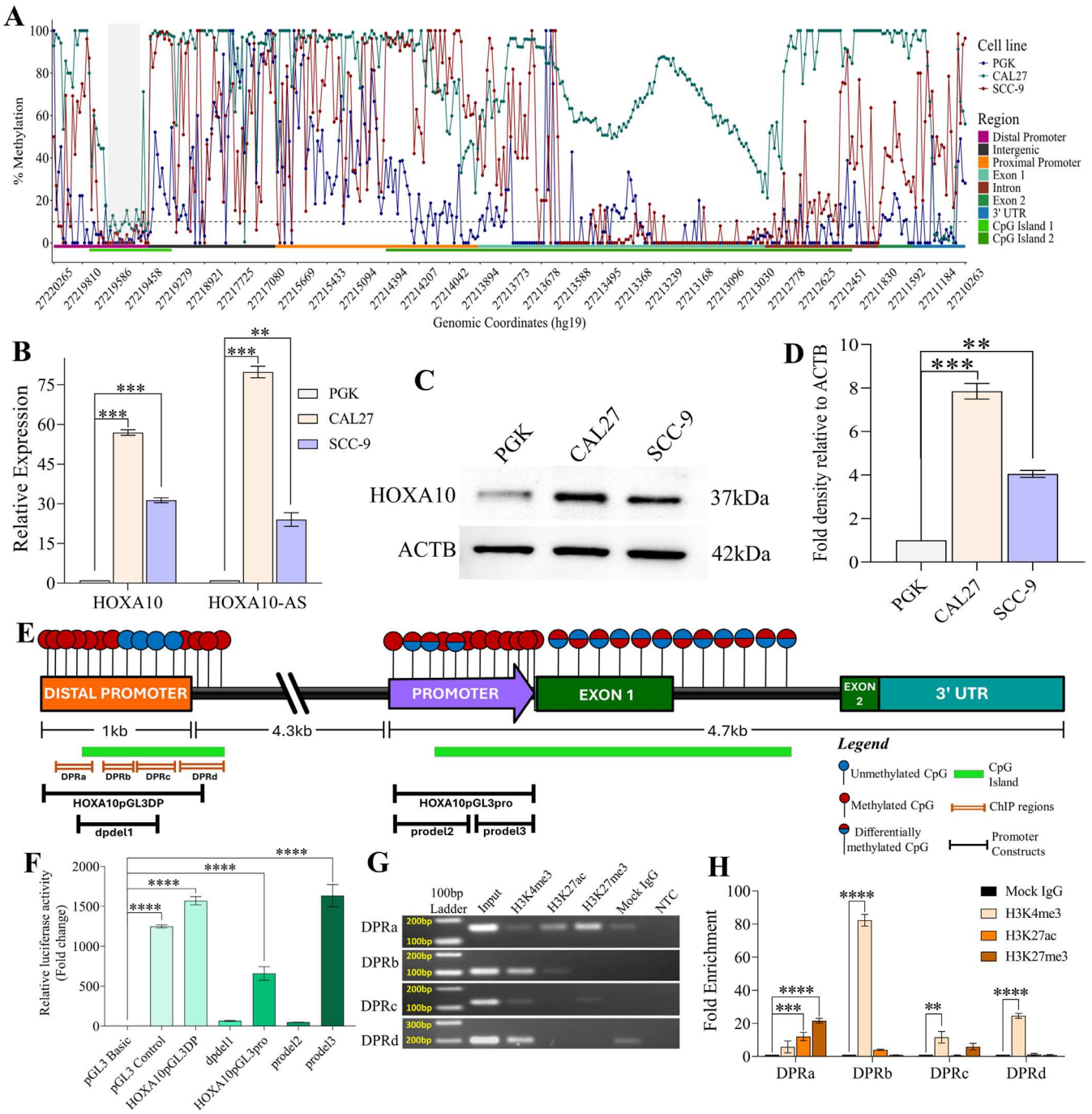

FIGURE 3 | Epigenetic regulation of *HOXA10* in oral cancer cells. (A) *HOXA10* gene-wide methylation in oral cancer cells (CAL27 and SCC-9) and normal primary gingival keratinocyte (PGK) cells. (B) Real-time PCR analysis of *HOXA10* and *HOXA10-AS* expression in CAL27 and SCC-9 cells compared with that in PGK cells. (C) Representative western blot images of *HOXA10* protein levels. ACTB was used as a loading control. (D) Densitometric quantification of *HOXA10* protein expression in oral cancer cells normalized to that in ACTB cells compared with that in PGK cells. The data are presented as the mean ± standard deviation derived from two biological replicates. Statistical significance was determined using two-tailed paired *t* tests (**$p < 0.01$; ***$p < 0.001$). (E) Graphical visualization of the *HOXA10* distal and proximal promoters and the design of promoter constructs and ChIP–qPCR primers on the basis of clinical sample methylation analysis and CpG island distribution. (F) Promoter activity is represented as relative light units (Fluc/Rluc) normalized to the internal control, pGL3 basic. (G) Gel analysis of histone enrichment in the distal promoter region via ChIP–qPCR. (H) Quantification of histone enrichment normalized to that of mock IgG, expressed as relative fold enrichment. One-way ANOVA with post hoc Tukey's test was used to determine the significance (*$p_{adj} < 0.05$; **$p_{adj} < 0.01$; ***$p_{adj} < 0.001$; ****$p_{adj} < 0.0001$).

constitutively methylated CpGs in both the patient and cell line methylation profiles irrespective of sample type, indicating a poised euchromatin state (Figure 3G,H). These results suggest that *HOXA10* regulation involves DNA methylation of the first exon and H3K4me3-enriched open chromatin in the distal promoter.

3.4 | Functional Analysis of NAT-Mediated Regulation of *HOXA10-AS* in OSCC

Transcript mapping of the *HOXA10-AS* splice variants to the genome revealed their anti-sense binding potential to the *HOX* genes *POU3F2* (POU class 3 homeobox 2), *HOXA9* (homeobox A9), *HOXD13* (homeobox D13), and *HOXA10* (homeobox A10). Genes such as *CARM1* (coactivator associated arginine methyltransferase 1), *ARID1B* (AT-rich interaction domain 1B), *CHD7* (chromodomain helicase DNA binding protein 7), and *NAT8L* (N-acetyltransferase 8 like) are involved in chromatin modifications, whereas *MAP6* (microtubule associated protein 6) and *KRT13* (keratin 13) play roles in the structure and cytoskeleton (Figure 4A). The protein–protein interaction network of genes regulated by *HOXA10-AS* revealed strong interactions with the *CREBBP* (CREB binding protein), *CARM1*, and *CHD7* genes. The *CREBBP* transcriptional coactivator is involved in cell cycle regulation, whereas *CARM1*, a coactivator of arginine methyltransferase, and *CHD7*, a chromodomain helicase transcription factor, are involved in chromatin remodeling (Figure 4B). GO terms related to BPs revealed significant ($p_{adj} < 0.05$) enrichment in response to DNA damage, chromatin remodeling, epithelial to mesenchymal regulation, cell proliferation, the G1/S-phase of the cell cycle checkpoint, and the regulation of RNA splicing (Figure 4C). KEGG pathway analysis revealed significant ($p_{adj} < 0.05$) hits in key cellular pathways, such as the p53 signaling, cell cycle, Wnt, TGFB, NFKB, and PI3k-Akt pathways (Figure 4D). These results implicate the regulation of cellular signaling pathways upon the modulation of *HOXA10-AS* antisense targets in OSCC owing to disease progression.

3.5 | Knockdown of *HOXA10-AS* Decreases the Expression of Its Antisense Target, *HOXA10*

A differential exon-specific siRNA design approach across the *HOXA10-AS* transcript was used to determine the effect of *HOXA10-AS* regulation (Figure 1A). *HOXA10-AS* expression was significantly ($F = 71.17$, $p = 0.0001$) lower in the siEx2 (0.24 ± 0.04, $q = 10.33$, $p = 0.0004$) and siEx3 (0.23 ± 0.03, $q = 10.51$, $p = 0.0004$) knockdown CAL27 cells than in the control cells. *HOXA10*, which is naturally antisense to the targeted *HOXA10-AS* gene, was significantly ($F = 63.56$, $p = 0.0002$) decreased in the siEx2 (0.30 ± 0.065, $q = 10.21$, $p = 0.0005$) and siEx3 (0.32 ± 0.084, $q = 9.98$, $p = 0.0005$) CAL27 cells (Figure 4E) due to *HOXA10-AS* knockdown. This was reflected in the significant ($F = 147.1$, $p = 0.0001$) reduction in the HOXA10 protein levels in both the siEx2 (0.29 ± 0.018, $q = 15.85$, $p = 0.0001$), siEx3 (0.24 ± 0.033, $q = 17.11$, $p = 0.0001$), and pooled siEx23 (0.42 ± 0.057, $q = 13.07$, $p = 0.0002$) CAL27 cells due to RNAi-mediated silencing of *HOXA10-AS* (Figure 4F,G) across the targeted exons of the *HOXA10-AS* transcript. Similar observations were also noted in the clinical patient cohorts analyzed in this study, where *HOXA10* and *HOXA10-AS* lncRNAs showed similar expression patterns (Figure 1B,C).

3.6 | Knockdown of *HOXA10-AS*-Reduced Cell Proliferation and Cell Migration, and Induced G1/S-Phase Arrest

Functional assays were performed using the siRNA targeting *HOXA10-AS* Exon 3 (siEx3) knockdown CAL27 cells, which are naturally sensitive to the target *HOXA10* gene (Figure 1A). Compared with that of the negative control (1.66 ± 0.15), the proliferation of the HOXA10-AS-knockdown CAL27 cells (0.98 ± 0.17, $t = 7.57$, $p = 0.0031$) was significantly lower (Figure 5A). Compared with the negative control (68.63 ± 0.74, 24.71 ± 0.02), cell cycle analysis revealed significantly increased accumulation of *HOXA10-AS*-knockdown cells in the G1 phase (75.48 ± 0.62, $t = 9.99$, $p = 0.009$), with unchanged S phase and decreased G2 phase ($18.99 \pm 0.99 \pm 0.48$, $t = 16.82$, $p = 0.0035$), suggesting G0/G1 or G1–S phase of cell cycle arrest (Figure 5B,C). A wound healing assay revealed significantly diminished wound closure (3.76 ± 1.93, $t = 11.99$, $p = 0.0001$) and a reduced cell migration rate (4.96 ± 0.42, $t = 36.7$, $p = 0.0019$) in the *HOXA10-AS* knockdown CAL27 cells compared with the negative control cells (32.43 ± 3.92, 8.43 ± 0.41) (Figure 5D–F). These results suggest the functional role of *HOXA10-AS* in regulating cell proliferation, migration, and the cell cycle in OSCC progression.

3.7 | *HOXA10-AS* Knockdown Deregulated the Cell Cycle, EMT, and Cell Signaling Pathways

Cell cycle markers such as CDKN1A (0.33 ± 0.04, $t = 19.35$, $p = 0.0027$), CDK2 (0.54 ± 0.075, $t = 24.80$, $p = 0.025$), and CDK6 (0.50 ± 043, $t = 7.29$, $p = 0.08$) were downregulated in the *HOXA10-AS*-knockdown CAL27 cells compared with the control cells (Figure 5G,H). The reduced CDK2 and CDK6 protein levels coincided with the G0/G1 or G1–S phase of cell cycle arrest observed (Figure 5B,C). CCNB1 (0.73 ± 0.19, $t = 8.66$, $p = 0.07$) was downregulated specifically in response to Exon 3 knockdown in *HOXA10-AS*, whereas CCND1 (1.67 ± 0.36) and CDH1 (1.50 ± 0.52) presented altered expression patterns due to Exon 2 knockdown in *HOXA10-AS*. A significant reduction in total CTNNB1 (0.42 ± 0.05, $t = 111.59$, $p = 0.007$) and LEF1 (0.29 ± 0.02, $t = 16.14$, $p = 0.003$) indicated decreased beta-catenin pathway activity (Figure 5I,J). The significantly reduced c-Met (0.53 ± 0.05, $t = 9.64$, $p = 0.01$), CDH2 (0.28 ± 0.15, $t = 5.97$, $p = 0.02$), and VIM (0.26 ± 0.07, $t = 10.60$, $p = 0.008$) levels indicate diminished EMT transition owing to the repression of *HOXA10-AS* (Figure 5K,L). These results highlight the exon-specific antisense-mediated regulation of *HOXA10-AS* on target genes, which affects OSCC progression.

4 | Discussion

Regulation mediated by NATs through lncRNAs represents a complex layer of gene control, contributing to the intricate network of molecular interactions that control gene expression. The dysregulation of NATs and their associated targets has been linked to cancer progression, where aberrant lncRNA expression can trigger unchecked cell proliferation and metastasis [6, 8, 9]. The lncRNA *HOXA10*-AS, which is located on the forward strand of Chromosome 7 (p15.2), is a NAT of *HOXA10*, which is located on the reverse strand. The last exon of all three *HOXA10*-AS transcript variants is complementary to the second exon of all five *HOXA10* gene transcript variants. *HOXA10-AS* has garnered attention for its role in the regulation of gene expression and its involvement in cancer biology [6]. Transcribed from the complementary strand to the *HOXA10* gene, it contributes to a complex network influencing *HOXA10* expression and related genes through natural antisense binding, thereby

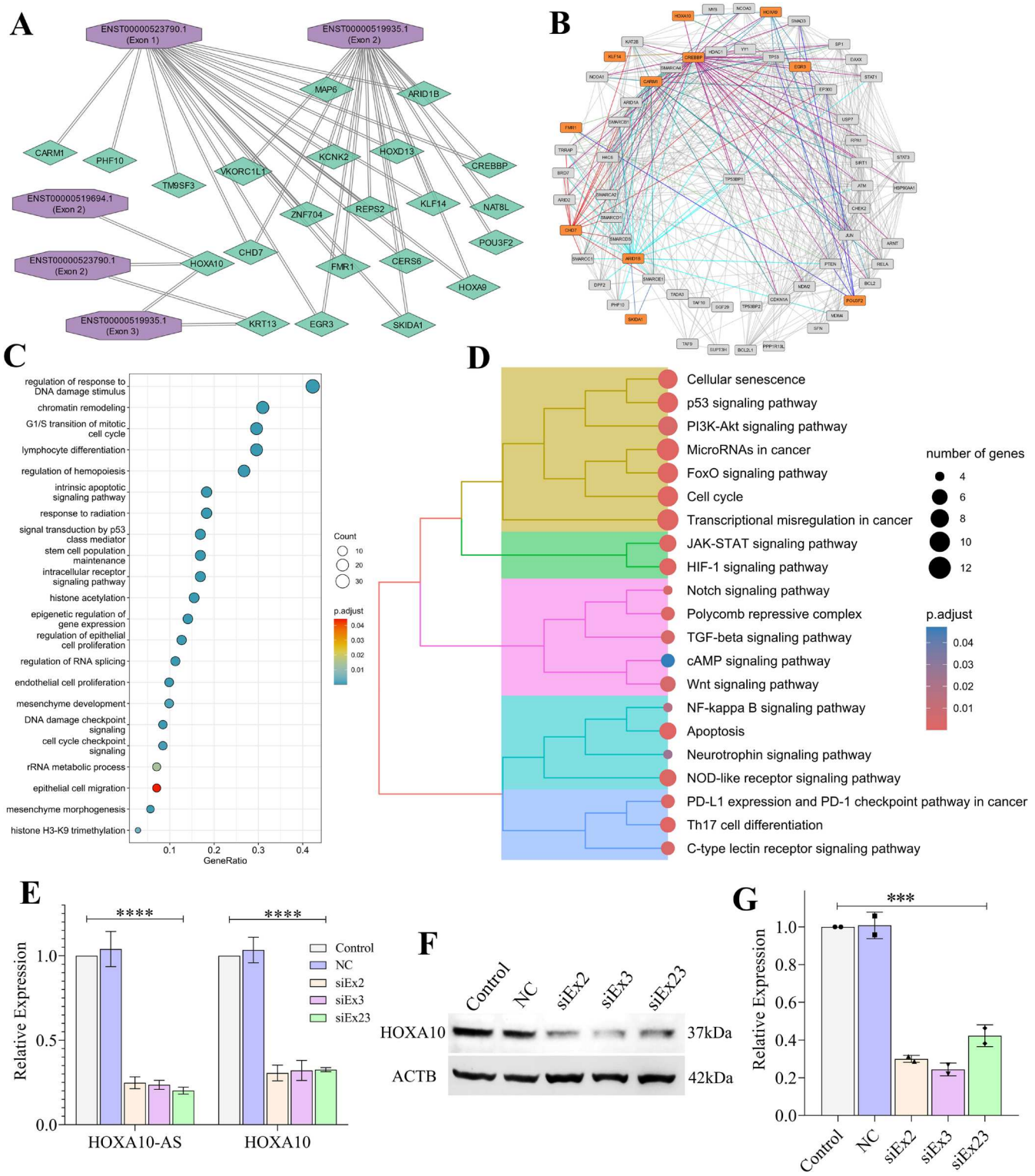

FIGURE 4 | Downstream molecular interactions and knockdown of *HOXA10-AS* in oral cancer cells. (A) Genome-wide antisense targets of the exonic regions of the lncRNA *HOXA10-AS* transcripts. (B) Protein–protein interaction network of *HOXA10-AS* antisense target genes predicted from StringDB (CS > 0.4). Orange-colored genes are the source genes. Functional enrichment analysis of *HOXA10-AS* antisense targets using (C) GO (biological process) and (D) KEGG pathway analyses was performed via the clusterProfiler R package. A Bonferroni–Hochberg adjusted p value of < 0.05 was considered to indicate statistical significance. (E) Expression of *HOXA10-AS* and its antisense target, *HOXA10*, was analysed using RT-qPCR, post siRNA-mediated knockdown of *HOXA10-AS*. (F) Western blot and (G) densitometric quantification of HOXA10 protein levels via NIH ImageJ. ACTB was used as a loading control. Statistical significance was determined using one-way ANOVA with post hoc Dunnett's test (*$p_{adj} < 0.05$; **$p_{adj} < 0.01$; ***$p_{adj} < 0.001$; ****$p_{adj} < 0.0001$). Control, untreated cells; NC, cells treated with negative control siRNA; siEx23, siRNAs targeting both Exons 2 and 3; siEx2, Exon 2-targeting siRNA; siEx3, Exon 3-targeting siRNA.

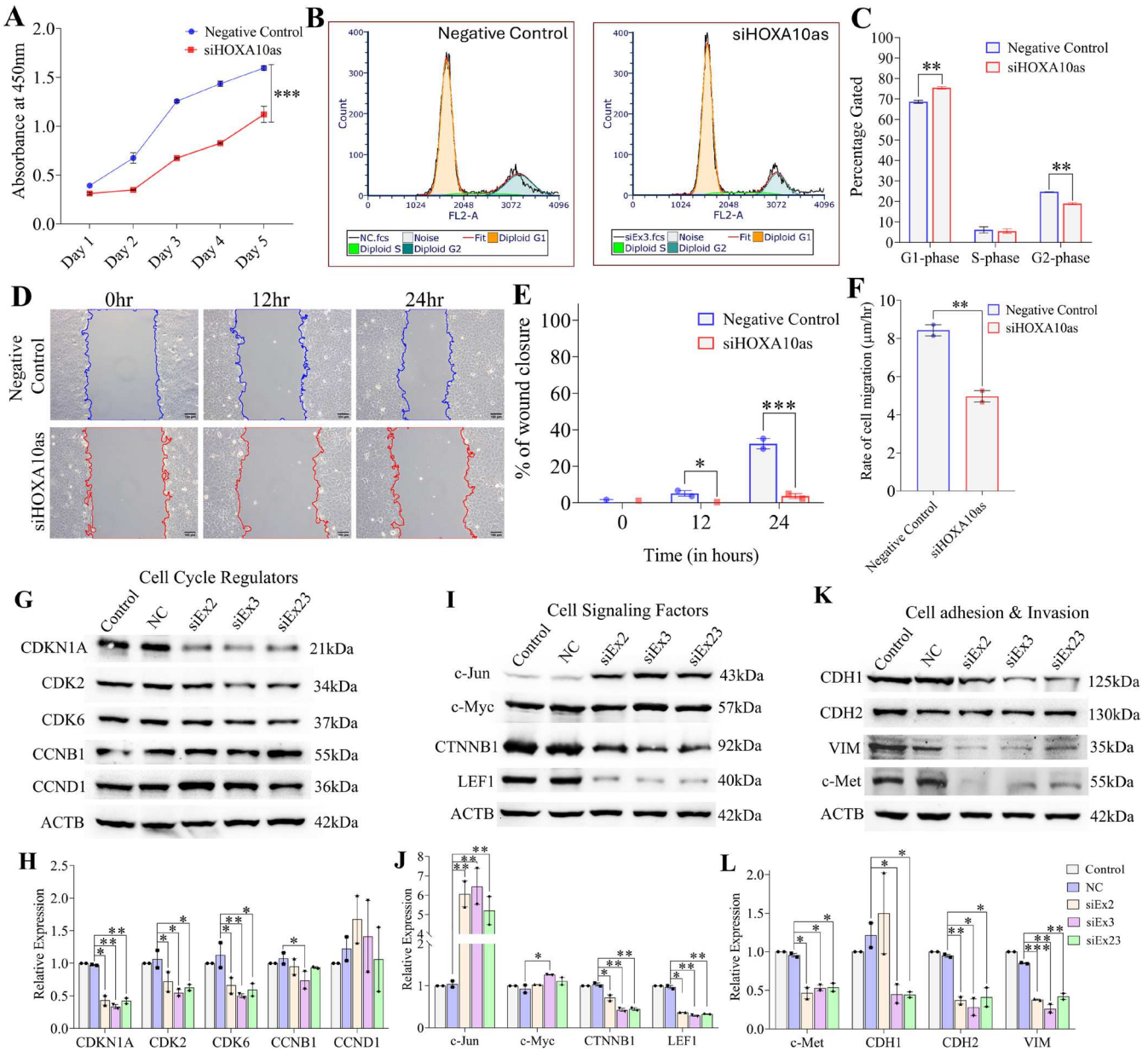

FIGURE 5 | *HOXA10-AS* dysregulates the cell cycle, beta-catenin and EMT in oral cancer cells. (A) Cell proliferation assay, (B, C) flow cytometry-based cell cycle analysis, (D–F) wound healing assay–wound closure and migration rates of *HOXA10-AS*-knockdown cells. Western blot and densitometric quantification of markers analysed in the (G, H) cell cycle, (I, J) cell signaling and (K, L) epithelial-to-mesenchymal transition upon exon-specific targeted knockdown of *HOXA10-AS* lncRNA. ACTB was used as a loading control, and protein expression was determined relative to the negative control. Statistical significance was assessed using a two-tailed paired or unpaired *t* test (*$p < 0.05$; **$p < 0.01$; ***$p < 0.001$). Negative control (NC), cells transfected with mock siRNA; siHOXA10as, targeted silencing of Exon 3 of *HOXA10-AS*.

affecting expression. *HOXA10* itself is pivotal for endometrial development and cellular differentiation [27], and its dysregulation is linked to various malignancies [6, 10, 11].

In OSCC, *HOXA10* overexpression is negatively correlated with patient survival and has prognostic implications [12]. Clinically, the increased expression of *HOXA10* and *HOXA10-AS* with increasing stage of OSCC progression, especially in lymph node-positive patients, suggests that *HOXA10* and *HOXA10-AS* play a role in cancer cell growth and metastasis [8, 28]. The expression of *HOXA10-AS* has been reported to be closely associated with cancer cell viability, and its overexpression is correlated with poor overall survival in oral cancer patients [8]. The upregulation of *HOXA10*-AS and *HOXA10* in OSCC samples, with higher expression in lymph node-positive samples and increasing expression with disease stage, suggests a regulatory relationship between these two genes at the RNA level. This finding indicates potential heterogeneity in *HOXA10* regulation by *HOXA10-AS* in OSCC progression.

The regulatory mechanisms of the *HOXA10* gene are evident in its distal and proximal promoters, which are rich in CpG sites and crucial for its transcriptional activity. Our analysis revealed that *HOXA10* was methylated in its first exon, which corresponded to decreased expression, suggesting epigenetic regulation by DNA methylation. Methylation in the first exonic

region of the gene body is associated with gene transcriptional silencing [29]. Moreover, our study revealed no significant differences in the methylation patterns of the *HOXA10-AS* NATs, likely because fewer methyl CpG probes were assayed in this region, which were mainly on the negative strand. This discrepancy does not conclusively indicate overall variation.

Additionally, *HOXA10* displayed a CUR in the CpG island located in the distal promoter region. The CURs [17] encompassed by a DMVs [18] in the surrounding region are characterized by abrupt decreases in the order of methylation across the region. The lack of methylation ensures that the DNA is probably in an open or euchromatin state, which is accessible to the transcription machinery, thereby promoting gene expression. CURs, particularly, when located in gene promoters or enhancers, enable the binding of regulatory proteins necessary for enhancing transcription. CURs regulate the stable expression of genes involved in developmental and fundamental cellular processes. CURs in developmental genes ensure that these genes are active when needed and can respond promptly to developmental cues owing to their unmethylated state. CURs are less likely to undergo aberrant hypermethylation, which can lead to the activation of oncogenes or the silencing of tumor suppressors. Therefore, these regions could play a protective role against inappropriate gene silencing, which could contribute to disease progression.

The region located 6.3 kb upstream of the gene body displayed H3K4me3 marks flanking either side of the unmethylated region, possibly indicating the presence of poised or active enhancer marks and a euchromatin state [30]. The high promoter activity, coupled with the enrichment of the histone marks H3K27ac and H3K4me3, highlights an active transcriptional state in these regions. Previous reports have indicated increased transcriptional activity in the distal region of the *HOXA10* promoter [31], a finding that is consistent with our study. Coupled with DNA epigenetics in the first exon, the distal promoter may increase promoter activity, contributing to *HOXA10* overexpression in OSCC.

Our analysis revealed that *HOXA10-AS* transcripts could interact with several homeobox genes, including *HOXA10*, and key genes involved in chromatin modifications and structural functions. Significant protein interactions with CREBBP, CARM1, and CHD7 affect cell cycle regulation and chromatin remodeling, impacting processes such as EMT and various signaling pathways. Targeted knockdown of *HOXA10-AS* exons in OSCC cells differentially impacts cell cycle regulation, EMT, and the beta-catenin pathway. Knockdown altered cell cycle progression by upregulating cyclin D1 and downregulating CDK2 (cyclin-dependent kinase 2), CDK6 (cyclin-dependent kinase 6), CCNB1, and CDKN1A (cyclin-dependent kinase inhibitor 1A) while inhibiting EMT progression by downregulating CTNNB1 (catenin beta 1), LEF1 (lymphoid enhancer binding factor 1), c-Met (proto-oncogene, receptor tyrosine kinase), CDH2 (N-cadherin), and VIM (vimentin).

The differential exon-specific regulation mediated by *HOXA10-AS* suggests its influence on key cell cycle markers, such as CCNB1 and CCND1, alongside the epithelial marker CDH1. This interplay highlights its potential to disrupt cell cycle control and epithelial integrity, which are critical hallmarks of cancer progression. Clinically, these findings could pave the way for targeting *HOXA10-AS* as a strategy to modulate cell cycle dysregulation and inhibit tumor progression in OSCC.

CDKN1A is responsible for encoding the p21 protein and crucially regulates the cell cycle by inhibiting cyclin-dependent kinases (CDKs). CDKN1A is a transcriptional target of the HOXA10 TF [32]. This could account for the observed reduction in the activity following decreased *HOXA10* expression due to effective *HOXA10-AS* knockdown in OSCC cells. Moreover, CDKN1A, which is a downstream target of CREBBP, a cAMP-response element binding protein (CREB) involved in transcriptional coactivation, was found to be targeted by *HOXA10-AS* Exon 2 via antisense-mediated regulation. These findings suggest that targeting *HOXA10-AS* influences critical cellular pathways that drive OSCC progression.

In summary, *HOXA10-AS* and *HOXA10* are upregulated in OSCC, with significant overexpression observed in lymph node-positive patients. *HOXA10-AS*, which functions as a NAT to *HOXA10*, showed similar expression patterns, suggesting NAT-mediated regulation. Enhanced *HOXA10* transcriptional activity occurs distally through histone modifications and proximally via promoter-driven first exon methylation. Knockdown of *HOXA10-AS* results in deregulation of the cell cycle, beta-catenin, and EMT transition. The effects of exon-specific knockdown of *HOXA10-AS* vary because of its intricate association with downstream targets through antisense-mediated regulation. The ability of *HOXA10-AS* to modulate key oncogenic pathways makes it a compelling subject for further research aimed at developing targeted therapies. Uncovering the NAT-specific molecular mechanisms underlying *HOXA10-AS* function in cancer can provide valuable insights into treatment strategies.

Author Contributions

Kanaka Sai Ram Padam: conceptualization, methodology, formal analysis and investigation, writing – original draft preparation. **Satyajit Dey Pereira:** methodology, formal analysis and investigation, writing – original draft preparation. **Naveena A. N. Kumar:** formal analysis and investigation, writing – review and editing, resources. **Raghu Radhakrishnan:** conceptualization, methodology, formal analysis and investigation, writing – review and editing, funding acquisition, resources.

Acknowledgments

Dr. TMA Pai Scholarship (201700105)—Manipal Academy of Higher Education, ICMR-Senior Research Fellow (3/1/3/JRF-2019/HRD-053(29379)).

Ethics Statement

This study was performed in accordance with the principles of the Declaration of Helsinki. Approval was granted by the Institutional Ethics Committee of the Manipal Academy of Higher Education (IEC: 348/2018).

Consent

Informed consent was obtained from all individual participants included in the study.

Conflicts of Interest

The authors declare no conflicts of interest.

Data Availability Statement

The authors state that all the data necessary for confirming the conclusions presented in this article, and where applicable, the publicly archived dataset analyzed, is represented fully within the article or can be provided by the authors upon request.

Peer Review

The peer review history for this article is available at https://www.webofscience.com/api/gateway/wos/peer-review/10.1111/jop.13613.

References

1. H. Sung, J. Ferlay, R. L. Siegel, et al., "Global Cancer Statistics 2020: GLOBOCAN Estimates of Incidence and Mortality Worldwide for 36 Cancers in 185 Countries," *CA: A Cancer Journal for Clinicians* 71, no. 3 (2021): 209–249, https://doi.org/10.3322/caac.21660.

2. J. A. Valdez and M. T. Brennan, "Impact of Oral Cancer on Quality of Life," *Dental Clinics of North America* 62, no. 1 (2018): 143–154, https://doi.org/10.1016/j.cden.2017.09.001.

3. S. Gupta, R. Gupta, D. N. Sinha, and R. Mehrotra, "Relationship Between Type of Smokeless Tobacco & Risk of Cancer: A Systematic Review," *Indian Journal of Medical Research* 148, no. 1 (2018): 56–76, https://doi.org/10.4103/ijmr.IJMR_2023_17.

4. J. L. Rinn and H. Y. Chang, "Genome Regulation by Long Noncoding RNAs," *Annual Review of Biochemistry* 81, no. 1 (2012): 145–166, https://doi.org/10.1146/annurev-biochem-051410-092902.

5. M. A. Faghihi and C. Wahlestedt, "Regulatory Roles of Natural Antisense Transcripts," *Nature Reviews. Molecular Cell Biology* 10, no. 9 (2009): 637–643, https://doi.org/10.1038/nrm2738.

6. C. Y. Dong, J. Cui, D. H. Li, Q. Li, and X. Y. Hong, "HOXA10-AS: A Novel Oncogenic Long Non-Coding RNA in Glioma," *Oncology Reports* 40, no. 5 (2018): 2573–2583, https://doi.org/10.3892/or.2018.6662.

7. J. Kuai, K. Wu, T. Han, W. Zhai, and R. Sun, "LncRNA HOXA10-AS Promotes the Progression of Esophageal Carcinoma by Regulating the Expression of HOXA10," *Cell Cycle* 22, no. 3 (2023): 276–290, https://doi.org/10.1080/15384101.2022.2108633.

8. Y. T. Chen, C. H. Kan, H. Liu, et al., "Modular Scaffolding by lncRNA HOXA10-AS Promotes Oral Cancer Progression," *Cell Death & Disease* 13, no. 7 (2022): 629, https://doi.org/10.1038/s41419-022-05071-6.

9. L. Jiang and Q. Yang, "HOXA10 Enhances Cell Proliferation and Suppresses Apoptosis in Esophageal Cancer via Activating p38/ERK Signaling Pathway," *Open Medicine* 17, no. 1 (2022): 1750–1759, https://doi.org/10.1515/med-2022-0558.

10. Y. Zhang, J. Chen, S. S. Wu, et al., "HOXA10 Knockdown Inhibits Proliferation, Induces Cell Cycle Arrest and Apoptosis in Hepatocellular Carcinoma Cells Through HDAC1," *Cancer Management and Research* 11 (2019): 7065–7076, https://doi.org/10.2147/CMAR.S199239.

11. B. Li, H. Jin, Y. Yu, et al., "HOXA10 Is Overexpressed in Human Ovarian Clear Cell Adenocarcinoma and Correlates With Poor Survival," *International Journal of Gynecological Cancer* 19, no. 8 (2009): 1347–1352, https://doi.org/10.1111/IGC.0b013e3181a83f1d.

12. X. Yan, B. Cong, Q. Chen, et al., "Silencing lncRNA HOXA10-AS Decreases Cell Proliferation of Oral Cancer and HOXA10-Antisense RNA Can Serve as a Novel Prognostic Predictor," *Journal of International Medical Research* 48, no. 8 (2020): 300060520934254, https://doi.org/10.1177/0300060520934254.

13. M. B. Amin, F. L. Greene, S. B. Edge, C. C. Compton, D. R. Byrd, and D. P. Winchester, "The Eighth Edition AJCC Cancer Staging Manual: Continuing to Build a Bridge From a Population-Based to a More "Personalized" Approach to Cancer Staging," *CA: a Cancer Journal for Clinicians* 67, no. 2 (2017): 93–99, https://doi.org/10.3322/caac.21388.

14. W. Liu, Y. Xie, J. Ma, et al., "IBS: An Illustrator for the Presentation and Visualization of Biological Sequences," *Bioinformatics* 31, no. 20 (2015): 3359–3361, https://doi.org/10.1093/bioinformatics/btv362.

15. K. J. Livak and T. D. Schmittgen, "Analysis of Relative Gene Expression Data Using Real-Time Quantitative PCR and the 2(-Delta Delta C(T)) Method," *Methods* 25, no. 4 (2001): 402–408, https://doi.org/10.1006/meth.2001.1262.

16. S. Andrews, *FastQC: A Quality Control Tool for High Throughput Sequence Data* (Babraham Bioinformatics, 2010).

17. Y. Chen, C. E. Breeze, S. Zhen, S. Beck, and A. E. Teschendorff, "Tissue-Independent and Tissue-Specific Patterns of DNA Methylation Alteration in Cancer," *Epigenetics & Chromatin* 9, no. 1 (2016): 10, https://doi.org/10.1186/s13072-016-0058-4.

18. H. Al Adhami, A. F. Bardet, M. Dumas, et al., "A Comparative Methylome Analysis Reveals Conservation and Divergence of DNA Methylation Patterns and Functions in Vertebrates," *BMC Biology* 20, no. 1 (2022): 70, https://doi.org/10.1186/s12915-022-01270-x.

19. M. J. Goldman, B. Craft, M. Hastie, et al., "Visualizing and Interpreting Cancer Genomics Data via the Xena Platform," *Nature Biotechnology* 38, no. 6 (2020): 675–678, https://doi.org/10.1038/s41587-020-0546-8.

20. W. J. Kent, "BLAT—The BLAST-Like Alignment Tool," *Genome Research* 12, no. 4 (2002): 656–664, https://doi.org/10.1101/gr.229202.

21. D. Szklarczyk, A. L. Gable, D. Lyon, et al., "STRING v11: Protein-Protein Association Networks With Increased Coverage, Supporting Functional Discovery in Genome-Wide Experimental Datasets," *Nucleic Acids Research* 47, no. D1 (2019): D607–D613, https://doi.org/10.1093/nar/gky1131.

22. P. Shannon, A. Markiel, O. Ozier, et al., "Cytoscape: A Software Environment for Integrated Models of Biomolecular Interaction Networks," *Genome Research* 13, no. 11 (2003): 2498–2504, https://doi.org/10.1101/gr.1239303.

23. M. Kanehisa and S. Goto, "KEGG: Kyoto Encyclopedia of Genes and Genomes," *Nucleic Acids Research* 28, no. 1 (2000): 27–30, https://doi.org/10.1093/nar/28.1.27.

24. G. Yu, L. G. Wang, Y. Han, and Q. Y. He, "clusterProfiler: An R Package for Comparing Biological Themes Among Gene Clusters," *OMICS* 16, no. 5 (2012): 284–287, https://doi.org/10.1089/omi.2011.0118.

25. A. Suarez-Arnedo, F. Torres Figueroa, C. Clavijo, P. Arbeláez, J. C. Cruz, and C. Muñoz-Camargo, "An Image J Plugin for the High Throughput Image Analysis of In Vitro Scratch Wound Healing Assays," *PLoS One* 15, no. 7 (2020): e0232565, https://doi.org/10.1371/journal.pone.0232565.

26. C. A. Schneider, W. S. Rasband, and K. W. Eliceiri, "NIH Image to ImageJ: 25 Years of Image Analysis," *Nature Methods* 9, no. 7 (2012): 671–675, https://doi.org/10.1038/nmeth.2089.

27. Y. Gui, J. Zhang, L. Yuan, and B. A. Lessey, "Regulation of HOXA-10 and Its Expression in Normal and Abnormal Endometrium," *Molecular Human Reproduction* 5, no. 9 (1999): 866–873, https://doi.org/10.1093/molehr/5.9.866.

28. M. Carrera, C. C. Bitu, C. E. de Oliveira, et al., "HOXA10 Controls Proliferation, Migration and Invasion in Oral Squamous Cell Carcinoma," *International Journal of Clinical and Experimental Pathology* 8, no. 4 (2015): 3613–3623, http://www.ncbi.nlm.nih.gov/pubmed/26097543.

29. F. Brenet, M. Moh, P. Funk, et al., "DNA Methylation of the First Exon Is Tightly Linked to Transcriptional Silencing," *PLoS One* 6, no. 1 (2011): e14524, https://doi.org/10.1371/journal.pone.0014524.

30. M. G. Guenther, S. S. Levine, L. A. Boyer, R. Jaenisch, and R. A. Young, "A Chromatin Landmark and Transcription Initiation at Most Promoters in Human Cells," *Cell* 130, no. 1 (2007): 77–88, https://doi.org/10.1016/j.cell.2007.05.042.

31. M. Mustafa, J. Y. Lee, and M. H. Kim, "CTCF Negatively Regulates HOXA10 Expression in Breast Cancer Cells," *Biochemical and Biophysical Research Communications* 467, no. 4 (2015): 828–834, https://doi.org/10.1016/j.bbrc.2015.10.058.

32. V. C. Bromleigh and L. P. Freedman, "p21 Is a Transcriptional Target of HOXA10 in Differentiating Myelomonocytic Cells," *Genes & Development* 14, no. 20 (2000): 2581–2586, https://doi.org/10.1101/gad.817100.

Supporting Information

Additional supporting information can be found online in the Supporting Information section.